

Sympathetic cooling of levitated optomechanics through nonreciprocal coupling

Jialin Li(李佳霖), Guangyu Zhang(张光宇), and Zhang-Qi Yin(尹璋琦)
Citation: Chin. Phys. B, 2026, 35 (**5**): 053701. DOI: 10.1088/1674-1056/ae4b25
http://cpb.iphy.ac.cn; http://iopscience.iop.org/cpb

What follows is a list of articles you may be interested in

Numerical analysis of motional mode coupling of sympathetically cooled two-ion crystals

Li-Jun Du(杜丽军), Yan-Song Meng(蒙艳松), Yu-Ling He(贺玉玲), and Jun Xie(谢军)
Chin. Phys. B, 2021, 30 (**7**): 073702. DOI: 10.1088/1674-1056/abfc3e

Simulation and experiment of the cooling effect of trapped ion by pulsed laser

Chang-Da-Ren Fang(方长达人), Yao Huang(黄垚), Hua Guan(管桦), Yuan Qian(钱源), and Ke-Lin Gao(高克林)
Chin. Phys. B, 2021, 30 (**7**): 073701. DOI: 10.1088/1674-1056/abf91f

Efficient loading of ultracold sodium atoms in an optical dipole trap from a high power fiber laser

Jing Xu(徐静), Wen-Liang Liu(刘文良), Ning-Xuan Zheng(郑宁宣), Yu-Qing Li(李玉清), Ji-Zhou Wu(武寄洲), Peng Li (李鹏), Yong-Ming Fu(付永明), Jie Ma(马杰), Lian-Tuan Xiao(肖连团), and Suo-Tang Jia(贾锁堂)
Chin. Phys. B, 2021, 30 (**3**): 033701. DOI: 10.1088/1674-1056/abc678

Ground state cooling of an optomechanical resonator with double quantum interference processes

Shuo Zhang(张硕), Tan Li(李坦), Qian-Hen Duan(段乾恒), Jian-Qi Zhang(张建奇), and Wan-Su Bao(鲍皖苏)
Chin. Phys. B, 2021, 30 (**2**): 023701. DOI: 10.1088/1674-1056/abc2c0

Development of adjustable permanent magnet Zeeman slowers for optical lattice clocks

Xiao-Hang Zhang(张晓航), Xin-Ye Xu(徐信业)
Chin. Phys. B, 2017, 26 (**5**): 053701. DOI: 10.1088/1674-1056/26/5/053701

RAPID COMMUNICATION

Sympathetic cooling of levitated optomechanics through nonreciprocal coupling

Jialin Li(李佳霖), Guangyu Zhang(张光宇), and Zhang-Qi Yin(尹璋琦)[†]

Center for Quantum Technology Research and Key Laboratory of Advanced Optoelectronic Quantum Architecture and Measurements (MOE), School of Physics, Beijing Institute of Technology, Beijing 100081, *China*

(Received 4 December 2025; revised manuscript received 21 February 2026; accepted manuscript online 27 February 2026)

Optomechanical cooling of levitated nanoparticles has become an essential topic in modern quantum physics, providing a platform for exploring macroscopic quantum phenomena and high-precision sensing. However, conventional cavity-assisted cooling is fundamentally constrained by cavity dissipation and environmental noise, limiting the attainable minimum temperature. In this work, we propose a non-Hermitian optomechanical cooling scheme through nonreciprocal coupling between two levitated nanoparticles, where one particle is directly cooled by an optical cavity and the other is cooled indirectly through a non-Hermitian interaction. Both analytical solutions and numerical simulations reveal that increasing nonreciprocity enhances directional energy transfer, enabling the target particle to reach a lower phonon occupation than is achievable in conventional cavity cooling. Theoretically, the nonreciprocal coupling scheme achieves a reduction in the steady-state phonon occupation number of the target particle by approximately 80% compared to the conventional cavity cooling limit. This study demonstrates a new cooling mechanism driven by non-Hermitian interactions, offering theoretical guidance for realizing controllable energy flow and deep cooling in levitated optomechanical systems and paving the way for future developments in quantum control and sensing technologies.

Keywords: levitated optomechanics, nonreciprocal coupling, laser cooling

PACS: 37.10.Vz, 87.80.Cc, 42.50.Wk, 42.50.Ct

DOI: 10.1088/1674-1056/ae4b25 **CSTR:** 32038.14.CPB.ae4b25

1. Introduction

Optomechanics, which explores the interaction between optical fields and mechanical motion, has emerged as a pivotal platform for realizing fundamental quantum control and precision measurement at the mesoscopic scale.[1,2] It plays a central role in diverse applications, such as optical cooling, quantum-state manipulation, and high-sensitivity force detection. Without efficient cooling, thermal noise dominates the dynamics of levitated nanoparticles, masking quantum behavior and limiting the sensitivity of force measurements. Conversely, once cooled to near their quantum ground state, these nanoparticles can exhibit macroscopic quantum superpositions and enable ultra-precise sensing beyond the standard quantum limit.[3]

In recent years, optical trapping and manipulation of levitated nanoparticles have attracted increasing attention due to their exceptional isolation from the environment and potential for observing macroscopic quantum phenomena,[3,4] nonlinear dynamics,[5] and ultrasensitive metrology.[6,7] Various techniques have been developed to cool the motion of levitated nanoparticles. Cavity-assisted cooling, where particles are coupled to a high-finesse optical cavity, enables sideband cooling analogous to trapped ions.[3,8] Feedback cooling, either through parametric modulation of the trapping potential or via electric field feedback, provides an alternative approach that does not require cavity coupling.[9] Among these, cavity cooling has become a cornerstone method that enables the suppression of thermal motion through cavity-mediated energy dissipation.[3,8] Such schemes have been successfully implemented in a variety of systems, including levitated microspheres, nanoparticle arrays, and atomic ensembles, where the coupling between cavity and mechanical modes allows energy transfer from mechanical degrees of freedom to the optical field, effectively reducing the temperature of the particle mode.[9,10]

Despite these advances, the achievable cooling limit in conventional cavity optomechanics remains restricted by cavity losses, coupling strength, and the intrinsic properties of the mechanical element.[11,12] This "cooling limit" arises from the fundamental trade-off in cavity optomechanics: to achieve strong cooling, one requires high cavity finesse and strong optomechanical coupling, but these same conditions amplify unwanted heating effects from cavity dissipation and photon recoil. In the resolved-sideband regime, the minimum phonon occupancy is fundamentally bounded by $n_{\min} = (\gamma/4\omega_{\mathrm{m}})^2$ for large mechanical frequency ω_{m} and cavity decay rate γ, a limit imposed by the balance between cooling and heating processes.[12] In levitated systems, especially under ultra-

[†]Corresponding author. E-mail: zqyin@bit.edu.cn

© 2026 Chinese Physical Society and IOP Publishing Ltd. All rights, including for text and data mining, AI training, and similar technologies, are reserved.

high vacuum conditions, the final phonon occupation is typically further constrained by the balance between cavity dissipation and environmental noise.[3] These fundamental limitations have motivated the search for new cooling mechanisms that can surpass the traditional sideband or feedback cooling limits, including unconventional dissipative engineering and multi-mode strategies.[13,14]

Recently, the introduction of non-Hermitian physics into photonic and optomechanical systems has opened new avenues for controlling energy flow and dissipation. Non-Hermitian interactions, characterized by asymmetric or nonreciprocal coupling, can induce directional energy transport and an effective gain loss balance within composite systems. Nonreciprocal coupling refers to an asymmetric interaction where the coupling strength from mode 1 to mode 2 differs from that from mode 2 to mode 1 (i.e., $g_{12} \neq g_{21}$). This breaks time-reversal symmetry and can be achieved through various techniques, such as dynamic modulation, synthetic gauge fields, or dissipative coupling in optomechanical systems.[15,16] Unlike reciprocal coupling, which preserves energy exchange symmetry, nonreciprocal coupling creates a preferred direction for energy flow, analogous to a one-way valve for phonons or photons. Such interactions have enabled a range of intriguing phenomena, including unidirectional photon (phonon) transmission,[17–19] exceptional points,[20,21] and topological mode control.[19,22] However, their potential for manipulating thermalization processes and achieving deep cooling in mechanical systems has not yet been thoroughly explored. Recent theoretical proposals suggest exponentially enhanced cooling using non-Hermitian chains[23] and related reservoir-engineering approaches.[15,16]

In this work, we propose a scheme for sympathetic cooling through nonreciprocal coupling between two optically levitated nanoparticles. In our model, only one particle (the auxiliary particle) is directly coupled to an optical cavity, while the other particle (the target particle) interacts with the auxiliary particle through a nonreciprocal mechanical coupling. The cavity particle coupling enables standard optomechanical cooling for the auxiliary particle, while the non-Hermitian interparticle interaction allows directional energy transfer from the target particle to the auxiliary particle, effectively extending the cooling effect to the target particle. By adjusting the nonreciprocal interaction strength, we demonstrate that the target particle can reach a lower steady-state phonon number than would be achievable through direct cavity cooling alone.

The remainder of this paper is organized as follows. In Section 2, we present the model and the non-Hermitian Hamiltonian of the coupled system. In Section 3, we derive the analytical solution by first obtaining the cavity-induced effective damping and temperature of the auxiliary particle, and then incorporating them into a two-mode non-Hermitian model of the two particles. In Section 4, we perform numerical simulations based on the full master equation to investigate the dynamical cooling behavior and verify the analytical results. Finally, Section 5 concludes with a discussion of the implications of our findings and potential applications of non-Hermitian cooling in levitated optomechanics and quantum thermodynamic control.

2. The scheme

We consider two optically levitated nanoparticles coupled through a nonreciprocal interaction and an optical cavity coupled only to one of them, as shown schematically in Fig. 1. Each nanoparticle is confined by a linearly polarized Gaussian trapping laser and behaves as a quantum oscillator with frequencies ω_a and ω_b for particles A and B, respectively. An optical cavity mode with resonance frequency ω_c interacts with particle A through radiation pressure coupling. Particle B, in contrast, does not couple directly to the cavity field but interacts with particle A through a nonreciprocal coupling channel, which can be engineered by controlling the optical phase, laser wavelength, cavity geometry, and the spatial separation between the particles.

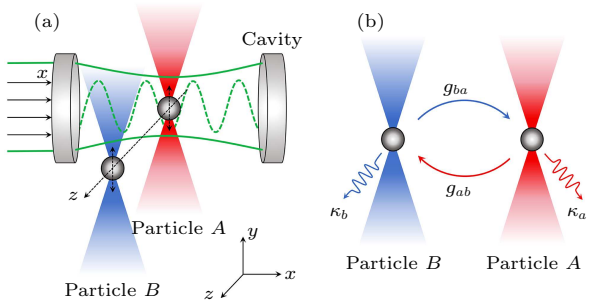


Fig. 1. (a) Schematic diagram of the nonreciprocal optomechanical cooling system. Particle A (shown in red) is optically trapped inside the cavity (shown in green) and coupled to the cavity mode through radiation pressure, while particle B (shown in blue) is levitated outside the cavity. Each particle supports a quantized harmonic mode with frequencies ω_a and ω_b, respectively. The coupling strengths are defined as $g_{ba} = g_1 + g_2$ (from particle B to A) and $g_{ab} = g_1 - g_2$ (from particle A to B). When $g_{ba} \neq g_{ab}$, nonreciprocal coupling is realized. (b) Illustration of the nonreciprocal coupling between particles A and B and their mechanical dissipation processes. The parameters κ_a and κ_b represent the mechanical damping rates of particles A and B, respectively, arising from their coupling to the thermal environment.

The total Hamiltonian of the system can be expressed as $H = H_0 + H_1$. The non-interaction part is given by $H_0 = \omega_c c^\dagger c + \omega_a a^\dagger a + \omega_b b^\dagger b$, where a ($a^\dagger$), b ($b^\dagger$), and c ($c^\dagger$) denote the annihilation (creation) operators of particle A, particle B, and the cavity mode, respectively. Meanwhile, ω_a and ω_b represent the mechanical oscillation frequencies of particles A and B, respectively. Physically, these frequencies are determined by the trapping potential curvature and the mass of the nanoparticles, typically ranging from tens of kHz to several MHz in typical levitated optomechanics experiments.[3] The parameter ω_c denotes the resonance frequency of the optical

cavity mode, which is set by the cavity length and determines the wavelength of light that can resonantly circulate within the cavity. H_1 describes the coupling between the two mechanical modes and the optomechanical interaction between particle A and the cavity,

$$H_1 = g_{ba}a^\dagger b + g_{ab}ab^\dagger + g(a^\dagger c + ac^\dagger), \tag{1}$$

where the coupling strengths are defined as $g_{ba} = g_1 + g_2$ (from particle B to A) and $g_{ab} = g_1 - g_2$ (from particle A to B). When $g_2 \neq 0$, we achieve $g_{ab} \neq g_{ba}$, realizing nonreciprocal coupling between the two nanoparticles. Here, g_1 represents the reciprocal coupling component, which arises from the conventional position–position interaction mediated by the optical field. The parameter g_2 denotes the nonreciprocal coupling component, which can be engineered through auxiliary driving fields, synthetic gauge fields, or dissipative coupling mechanisms that break time-reversal symmetry.[15,16,24–26] Physically, g_2 acts as the key control parameter that determines the directionality and strength of the energy flow between the two mechanical modes. The interaction becomes non-Hermitian when $\mathrm{Re}(g_2) \neq 0$, corresponding to unidirectional energy flow between the particles. The parameter g denotes the linearized coupling rate between particle A and the cavity field.

In a frame rotating at the driving laser frequency ω_L, the cavity frequency is replaced by the detuning parameter $\Delta = \omega_\mathrm{L} - \omega_c$, and the free Hamiltonian becomes $H_0' = -\Delta\, c^\dagger c + \omega_a a^\dagger a + \omega_b b^\dagger b$. The detailed derivation of this transformation, including the explicit use of the unitary operator $U(t) = \exp[\mathrm{i}\omega_\mathrm{L} t(c^\dagger c)]$ and the Baker–Campbell–Hausdorff formula,[1] is provided in Appendix A for completeness. This transformation eliminates the fast optical oscillations. Under the rotating-wave approximation, rapidly oscillating counter-rotating terms such as ac and $a^\dagger c^\dagger$ are neglected since their effects average out when the coupling strengths are small compared with the optical and mechanical frequencies. The effective Hamiltonian governing the system dynamics in the rotating frame is therefore[27,28]

$$\begin{aligned} H_\mathrm{eff} &= -\Delta\, c^\dagger c + \omega_a a^\dagger a + \omega_b b^\dagger b \\ &\quad + g_{ab}ab^\dagger + g_{ba}a^\dagger b + g(a^\dagger c + ac^\dagger). \end{aligned} \tag{2}$$

The detuned cavity mechanical coupling, the asymmetric inter-particle interaction, and the unidirectional phonon exchange characteristic of non-Hermitian dynamics are explicitly captured in Eq. (2).

Initially, both particle A and B are in the thermal states with the average thermal phonon number $\bar{n}_a$ and $\bar{n}_b$. We achieve cooling of the target particle B through the cavity and the auxiliary particle A. Considering the non-Hermitian interaction and the unavoidable intrinsic loss, the evolution of the whole system containing decay and damping can be described by the quantum master equation[29]

$$\begin{aligned} \dot{\rho}_\mathrm{sys} &= \mathcal{L}\rho_\mathrm{sys} \\ &= -\mathrm{i}(H_\mathrm{eff}\rho_\mathrm{sys} - \rho_\mathrm{sys}H_\mathrm{eff}^\dagger) + \mathrm{i}\mathrm{Tr}[\rho_\mathrm{sys}(H_\mathrm{eff} - H_\mathrm{eff}^\dagger)]\rho_\mathrm{sys} \\ &\quad + (\mathcal{L}_a + \mathcal{L}_b + \mathcal{L}_c)\rho_\mathrm{sys}, \end{aligned} \tag{3}$$

where the Lindblad superoperators are given by

$$\mathcal{L}_a = (1+\bar{n}_a)\kappa_a D_a + \bar{n}_a\kappa_a D_{a^\dagger}, \tag{4}$$

$$\mathcal{L}_b = (1+\bar{n}_b)\kappa_b D_b + \bar{n}_b\kappa_b D_{b^\dagger}, \tag{5}$$

$$\mathcal{L}_c = \gamma D_c. \tag{6}$$

Here, D_x refers to the notation in the Lindblad form, which is expressed as $D_x(\rho) = 2x\rho x^\dagger - x^\dagger x\rho - \rho x^\dagger x$. The trace-correction term $\mathrm{i}\mathrm{Tr}[\rho_\mathrm{sys}(H_\mathrm{eff} - H_\mathrm{eff}^\dagger)]\rho_\mathrm{sys}$ is introduced to guarantee trace preservation during non-Hermitian evolution. κ_a and κ_b are the mechanical decay rates of particle A and B, respectively, and γ is the intrinsic decay rate of the cavity. Equation (3) will be solved using both analytical and numerical methods, and the results will be discussed in the following sections.

3. Analytical solution

In this section, we derive the analytical expressions governing the steady-state phonon numbers of the two mechanical modes. Starting from the complete three-mode master equation presented in Section 2, we first obtain an effective description of particle A by treating the cavity–A subsystem as a linearized optomechanical pair. This allows us to identify an optically induced damping rate and an effective thermal occupation for mode a. We then incorporate these effective parameters into a reduced two-mode non-Hermitian model for particles A and B, from which closed dynamical equations for the phonon numbers can be obtained.

Throughout this section, we make use of the fact that, under the bad-cavity limit and the harmonic oscillator approximation, mode a is cooled to a sufficiently small amplitude such that the nonlinear trace-correction term $\mathrm{i}\mathrm{Tr}[\rho_\mathrm{sys}(H_\mathrm{eff} - H_\mathrm{eff}^\dagger)]\rho_\mathrm{sys}$ in the original master equation contributes negligibly to the dynamics (see Appendix B for the formal justification).

3.1. Effective bath description for particle A

We consider the coupled cavity–A subsystem prior to introducing particle B. In a frame rotating at the cavity drive frequency, the standard linearized optomechanical Hamiltonian reads[27,28]

$$H_{c-A} = -\Delta c^\dagger c + \omega_a a^\dagger a + g(a^\dagger c + ac^\dagger). \tag{7}$$

The cavity induces anti-Stokes and Stokes scattering rates

$$\Gamma_- = g^2 \frac{\gamma}{(\Delta - \omega_a)^2 + (\gamma/2)^2}, \tag{8}$$

$$\Gamma_+ = g^2 \frac{\gamma}{(\Delta+\omega_a)^2+(\gamma/2)^2}, \tag{9}$$

which respectively cool and heat the mechanical mode. The optically induced damping rate and effective occupation of the optical reservoir are therefore

$$\Gamma_{\rm opt} = \Gamma_- - \Gamma_+, \tag{10}$$

$$n_{\rm opt} = \frac{\Gamma_+}{\Gamma_- - \Gamma_+}. \tag{11}$$

Combining optical and intrinsic mechanical dissipation, the total effective damping rate and total effective bath occupation of particle A become

$$\kappa_a^{(\rm eff)} = \kappa_a + \Gamma_{\rm opt}, \tag{12}$$

$$\bar{n}_a^{(\rm eff)} = \frac{\kappa_a \bar{n}_a + \Gamma_{\rm opt} n_{\rm opt}}{\kappa_a^{(\rm eff)}}. \tag{13}$$

These expressions provide an explicit mapping from the physical cavity parameters (γ, Δ, g) to an effective thermal environment for particle A. For the convenience of the notation, we rename $\kappa_a^{(\rm eff)} \to \kappa_a'$ and $\bar{n}_a^{(\rm eff)} \to \bar{n}_a'$.

3.2. Two-mode non-Hermitian dynamics

With the cavity eliminated in favor of an effective bath for mode a, we now turn to the reduced two-mode system, which captures the essential non-Hermitian dynamics between particles A and B. The Hamiltonian is

$$H_{A-B} = \omega_a a^\dagger a + \omega_b b^\dagger b + g_{ab} a b^\dagger + g_{ba} a^\dagger b. \tag{14}$$

Mode a now couples to the effective bath characterized by $(\kappa_a', \bar{n}_a')$, while mode b retains its intrinsic dissipation $(\kappa_b, \bar{n}_b)$. The master equation for the reduced density matrix $\rho_{a,b}$ is

$$\begin{aligned} \dot{\rho}_{a,b} &= \mathcal{L}' \rho_{a,b} \\ &= -{\rm i}(H_{A-B}\rho_{a,b} - \rho_{a,b} H_{A-B}^\dagger) + (\mathcal{L}_a' + \mathcal{L}_b)\rho_{a,b}, \end{aligned} \tag{15}$$

where $\mathcal{L}_a' = (1+\bar{n}_a')\kappa_a' D_a + \bar{n}_a' \kappa_a' D_{a^\dagger}$.

Using the standard adjoint Liouville method,[29] we derive the equations of motion for the average phonon number. Applying the adjoint Liouvillian corresponding to Eq. (15) to the number operators $n_a = a^\dagger a$ and $n_b = b^\dagger b$ yields coupled nonlinear differential equations[13,14] (see Appendix C for the full derivation):

$$\begin{aligned} \frac{\rm d}{{\rm d}t} n_a &= \frac{2(g_1+g_2)^2}{\kappa_a'+\kappa_b}(1+n_a)n_b - \frac{2(g_1-g_2)^2}{\kappa_a'+\kappa_b} n_a (1+n_b) \\ &\quad + \kappa_a'(\bar{n}_a' - n_a), \\ \frac{\rm d}{{\rm d}t} n_b &= -\frac{2(g_1+g_2)^2}{\kappa_a'+\kappa_b}(1+n_a)n_b + \frac{2(g_1-g_2)^2}{\kappa_a'+\kappa_b} n_a (1+n_b) \\ &\quad + \kappa_b(\bar{n}_b - n_b). \end{aligned} \tag{16}$$

At the steady state, i.e., when ${\rm d}n_a/{\rm d}t = {\rm d}n_b/{\rm d}t = 0$, taking the quantum expectation values of both sides and employing the mean-field approximation $\langle n_a n_b \rangle = \langle n_a \rangle \langle n_b \rangle$, we can solve for the steady-state average phonon number of particle B from a quadratic equation written as

$$A\langle n_b \rangle^2 + B\langle n_b \rangle + C = 0, \tag{17}$$

with coefficients

$$A = \frac{8 g_1 g_2 \kappa_b}{\kappa_a'(\kappa_a'+\kappa_b)}, \tag{18a}$$

$$\begin{aligned} B = &-\frac{8 g_1 g_2}{\kappa_a'+\kappa_b}\left(\bar{n}_a' + \frac{\kappa_b}{\kappa_a'}\bar{n}_b\right) \\ &- \frac{2(g_1+g_2)^2}{\kappa_a'+\kappa_b} - \frac{2(g_1-g_2)^2}{\kappa_a'+\kappa_b}\cdot\frac{\kappa_b}{\kappa_a'} - \kappa_b, \end{aligned} \tag{18b}$$

$$C = \frac{2(g_1-g_2)^2}{\kappa_a'+\kappa_b}\left(\bar{n}_a' + \frac{\kappa_b}{\kappa_a'}\bar{n}_b\right) + \kappa_b \bar{n}_b. \tag{18c}$$

3.3. Steady-state phonon occupations

The steady-state average phonon number of particle A is derived analogously and provided in Appendix D. We numerically solved Eq. (16) for both particles, excluding nonphysical solutions, and analyzed the steady-state phonon populations $\langle n_a \rangle$ and $\langle n_b \rangle$ as functions of the nonreciprocal coupling parameter $K_g = (g_1+g_2)/(g_1-g_2)$ $(g_1 \neq g_2)$. This parameter characterizes the degree of nonreciprocity between particle A and particle B, with a larger K_g representing stronger unidirectional energy transfer from particle B to particle A within the same interaction timescale. Physically, $K_g > 1$ corresponds to the regime where the nonreciprocal component g_2 dominates over the reciprocal component g_1 in determining the directionality of energy flow. In this regime, the asymmetric coupling creates an effective directional channel that facilitates energy transfer from particle B to particle A, enabling cooling of the target particle beyond the conventional cavity cooling limit. As K_g increases, the degree of nonreciprocity becomes more pronounced, leading to more efficient directional energy transfer.

In our calculations, the characteristic mechanical frequency used lies in the range of 10^5–10^6 Hz, consistent with experimentally measured center-of-mass and torsional-mode frequencies of optically levitated nanoparticles in cavity and tweezer-based traps.[25,26] For convenience, all the parameters in the calculation are expressed in dimensionless units, where the mechanical frequencies are normalized as $\omega_a = \omega_b = \Delta = 1$. The cavity–$A$ coupling strengths $g = 0.01$–0.05 correspond to linearized optomechanical coupling rates of approximately 10^3–10^4 Hz, and the mechanical damping rates $\kappa_a = \kappa_b = 10^{-4}$ represent intrinsic line widths of 10–100 Hz typical for levitated nanoparticles at high vacuum. The thermal occupations $\bar{n}_a = \bar{n}_b = 20$ correspond to effective mode temperatures in the millikelvin regime following precooling through feedback or cavity-assisted schemes. Recent torsional-mode implementations have demonstrated that nonreciprocal mechanical coupling can reach relatively large

values of K_g,[25,26,30] highlighting the feasibility of accessing strongly asymmetric interaction regimes in experiments.

As shown in Fig. 2, the analytical steady-state solutions exhibit a clear dependence of the phonon populations on the degree of nonreciprocity. When the cavity–A coupling is relatively strong as in Fig. 2(a), particle A is efficiently cooled and therefore remains nearly insensitive to variations in K_g, whereas particle B experiences a pronounced reduction in its phonon number due to the increasingly directional energy flow from B to A. In contrast, for weaker cavity coupling as in Fig. 2(b), the reduced optical damping of particle A results in gradual phonon accumulation as K_g increases, while particle B still undergoes enhanced cooling under stronger nonreciprocity. In both regimes, the limit $K_g \to 1^+$ leads to $n_A \approx n_B$, consistent with the restoration of reciprocal coupling. Examining both Figs. 2(a) and 2(b), we find that at $K_g = 2.0$, the introduction of nonreciprocal coupling achieves a reduction in the steady-state phonon number of the target particle by approximately 80% compared to the reciprocal coupling case ($K_g \to 1^+$). These results collectively demonstrate that nonreciprocal interactions offer a robust mechanism for improving the remote cooling of particle B, with the behavior of particle A primarily governed by the strength of its cavity-induced dissipation.

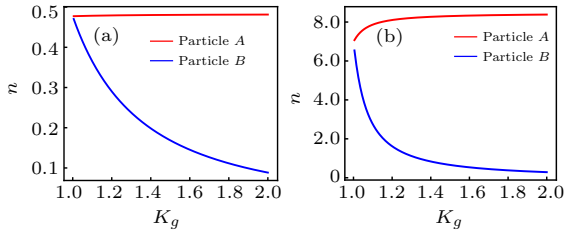


Fig. 2. Steady-state phonon numbers of particles A and B versus the nonreciprocal coupling parameter K_g. All parameters are expressed in dimensionless units with $\omega_a = \omega_b = \Delta = 1$. The remaining parameters are fixed as $\gamma = 1$, $\bar{n}_a = \bar{n}_b = 20$, $\kappa_a = \kappa_b = 10^{-4}$, and $g_2 = 0.1$. The nonreciprocal coupling coefficient is chosen as $g_1 = g_2(K_g+1)/(K_g-1)$ so that $K_g > 1$ corresponds to an increasingly nonreciprocal interaction. Particles A and B correspond to the red and blue lines, respectively. (a) Results for cavity–A coupling $g = 0.05$. Here n_A remains almost constant, while n_B decreases significantly with K_g due to efficient directional energy transfer into the strongly cooled particle A. (b) Results for weaker coupling $g = 0.01$. In this regime n_B continues to decrease exponentially with K_g, whereas n_A increases slowly and reaches values one order of magnitude larger than in that in panel (a), reflecting phonon accumulation at particle A. In both panels, n_A and n_B approach each other as $K_g \to 1^+$, consistent with the reciprocal coupling limit.

4. Numerical simulation

To verify the analytical results and investigate the dynamical cooling behavior of the coupled system, we numerically solve the full time-dependent master equation for the total density matrix $\rho_{\rm sys}(t)$ as described in Eq. (3). The time evolution of $\rho_{\rm sys}(t)$ is computed using the Runge–Kutta algorithm, which allows high-order integration accuracy and flexible adaptive time stepping. The Hilbert space of each mode is truncated to a finite dimension to ensure numerical convergence while keeping computational costs manageable.[29,31,32] The initial state is chosen as $|0\rangle_A|2\rangle_B|0\rangle_C$, corresponding to the case where only particle B initially possesses vibrational excitations, while particle A and the cavity mode are both in their ground states. This initial condition simulates a scenario where the target particle B is in a thermally excited state, while the auxiliary system (particle A and the cavity) has been precooled, allowing us to isolate the cooling dynamics driven by nonreciprocity. By initially placing all excitations in particle B, we can clearly observe how the nonreciprocal coupling facilitates directional energy transfer from the target particle to the auxiliary system, leading to sympathetic cooling of particle B without direct cavity interaction.

During the time evolution, we calculate the expectation values of the phonon number operators $n_A = {\rm Tr}[\rho_{\rm sys}a^\dagger a]$, $n_B = {\rm Tr}[\rho_{\rm sys}b^\dagger b]$, and $n_C = {\rm Tr}[\rho_{\rm sys}c^\dagger c]$ to monitor the cooling process of each mode.[33] To guarantee the physical validity of the simulation, the trace of $\rho_{\rm sys}$, the minimum diagonal element, and the smallest eigenvalue of its Hermitian part are also evaluated throughout the evolution to verify trace preservation, positivity, and numerical stability of the density matrix.[34,35]

In Fig. 3, time is scaled by the mechanical damping rate κ, where we have set $\kappa = \kappa_a = \kappa_b = 0.01$ in dimensionless units. As shown in Fig. 3, the time evolution of the phonon numbers for particles A and B under two distinct coupling conditions is plotted. In both cases, the system evolves from the initial nonequilibrium configuration toward a steady state, where the phonon populations of the two particles exhibit a clear asymmetry. The target particle B continuously loses energy to particle A through the nonreciprocal interaction channel, leading to a reduction in its steady-state phonon number. By contrast, particle A accumulates energy during the same process, resulting in an increased phonon occupation.

The comparison between Figs. 3(a) and 3(b) reveals that increasing the nonreciprocal parameter K_g not only enhances the unidirectional energy transfer but also substantially reduces the steady-state phonon population of the target particle B. The numerical simulations show that the nonreciprocal cooling scheme presented in Fig. 3(b) achieves approximately 40% reduction in the steady-state phonon number of the target particle compared to the reciprocal coupling case approximated by Fig. 3(a). Due to computational limitations that restrict the initial phonon occupation to relatively small values in our direct integration of the full master equation, this reduction is less pronounced than the 80% enhancement predicted by the analytical solutions under optimal parameter conditions. Although relatively small parameters are chosen here due to the numerical cost of directly integrating the full master equation after Hilbert-space truncation, the observed cooling contrast between different K_g values is already significant. Under

realistic experimental parameters with stronger coupling and higher cavity quality factors, the cooling asymmetry and overall reduction in $\langle n_B \rangle$ are expected to be even more pronounced. These results confirm that non-Hermitian interactions can effectively facilitate asymmetric energy dissipation and enable sympathetic cooling below the conventional optomechanical limits.

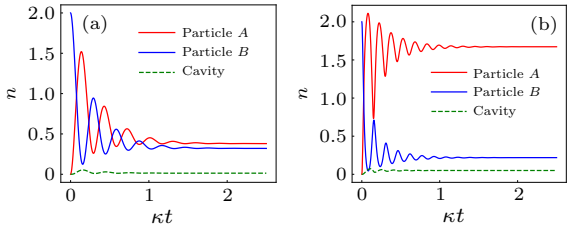


Fig. 3. Time evolution of the phonon number n for particles A and B. particle B is the target to be cooled, while particle A acts as the auxiliary system mediating the cooling process. The initial phonon numbers of particles A and B are 0 and 2, respectively. The parameters are $g = 0.1$, $\gamma = 1.0$, $\kappa = \kappa_a = \kappa_b = 0.01$, and $\bar{n}_a = \bar{n}_b = 1$. Particle A, B, and the cavity correspond to the red solid, blue solid, and green dashed lines, respectively. (a) $g_1 + g_2 = 0.11$, $g_1 - g_2 = 0.1$ ($K_g = 1.1$). The steady-state phonon numbers are $n_B = 0.32$ and $n_A = 0.38$. (b) $g_1 + g_2 = 0.40$, $g_1 - g_2 = 0.1$ ($K_g = 4.0$). The steady-state phonon numbers are $n_B = 0.22$ and $n_A = 1.69$. As K_g increases, the nonreciprocity strengthens, leading to lower n_B and higher n_A, which highlights the directional energy transfer and enhanced non-Hermitian cooling efficiency.

For larger parameter regimes where the Hilbert-space dimension becomes significantly larger, direct time-domain integration of the master equation is computationally demanding and memory-intensive. In this case, the steady-state phonon number is obtained by solving the stationary master equation $\mathcal{L}\rho_{\rm ss} = 0$ using sparse-matrix techniques.[31,32] Specifically, we construct the full Liouvillian superoperator $\mathcal{L}$ in the column-stacking representation,[36,37] where both coherent and dissipative contributions are included in a sparse compressed sparse row format. The steady-state density matrix $\rho_{\rm ss}$ is then determined by replacing one row of $\mathcal{L}$ with the trace constraint $\mathrm{Tr}(\rho_{\rm ss}) = 1$[38] and solving the resulting linear system. After the numerical solution is obtained, the density matrix is Hermitized and normalized to guarantee physical validity (trace preservation and positivity). The steady-state phonon numbers $\langle n_A \rangle$ and $\langle n_B \rangle$ are then computed from $\langle n_j \rangle = \mathrm{Tr}[\rho_{\rm ss} a_j^\dagger a_j]$ ($j = A, B$).

We have compared the analytical steady-state phonon occupations with the numerical results obtained from the full three-mode Liouvillian simulation, as shown in Fig. 4. In the weakly nonreciprocal regime, where K_g is only slightly above unity, the agreement between the two approaches is very good, confirming the consistency of the effective-bath reduction and the reduced two-mode non-Hermitian model. The deviation observed when $K_g > 1.25$ primarily stems from Hilbert space truncation, as the population of particle A becomes large in the strongly nonreciprocal regime. In this regime the truncated Hilbert space cannot fully capture the high-excitation tails, consistent with convergence diagnostics, although the numerically stable region still exhibits clear agreement with the theoretical trend. Fully handling higher excitations requires methods beyond the linearized model, such as matrix product states or full quantum master equation simulations with larger Hilbert space dimensions, marking an interesting region worthy of future study.

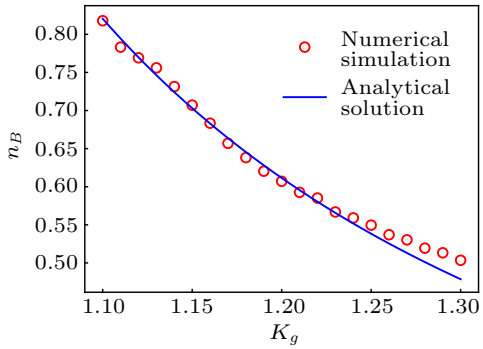


Fig. 4. Comparison between the analytical and numerical steady-state phonon numbers of particle B as a function of the nonreciprocal coupling parameter K_g. The red dots represent the results obtained from the sparse-Liouvillian steady-state solver, and the blue solid line shows the analytical solution based on Eq. (16). $g_2 = 0.1$, $g_1 = g_2(K_g + 1)/(K_g - 1)$, $g = 0.05$, $\kappa_a = \kappa_b = 10^{-4}$, $\gamma = 2$, and $\bar{n}_a = \bar{n}_b = 20$.

Beyond numerical truncation effects, it is important to note that such deviations may also signal the onset of additional physical mechanisms that are not fully captured by the analytical treatment. The analytical model relies on several controlled approximations, including linearized dynamics, effective bath elimination, and the neglect of higher-order correlations. When K_g becomes large, the strongly directional energy flow can substantially enhance fluctuations and occupation numbers in the auxiliary mode, potentially amplifying nonlinear optomechanical effects or inducing non-negligible quantum correlations between the two mechanical subsystems. Similar breakdowns of linearized or reduced descriptions at strong nonreciprocity or strong effective coupling have been discussed in related non-Hermitian and cascaded-system settings.[15,39] In particular, higher-order phonon processes, weak mechanical nonlinearities, or entanglement-induced backaction may modify the steady-state properties in ways that are not accounted for in the effective non-Hermitian Hamiltonian. From this perspective, the observed quantitative deviations at large K_g should not be interpreted solely as numerical artifacts, but rather as a potentially meaningful indicator of the limits of the present theoretical framework.

In conclusion, while the analytical model faithfully captures the key qualitative features of non-Hermitian cooling and its dependence on the nonreciprocity parameter K_g, a definitive identification of the origin of the deviations at strong nonreciprocity requires more refined theoretical models and further optimized numerical simulations with extended Hilbert

spaces. This regime therefore represents an interesting direction for future investigation.

5. Conclusion

We have theoretically proposed and analyzed a sympathetic cooling scheme through nonreciprocal coupling between two optically levitated nanoparticles. In this system, only one particle is directly coupled to an optical cavity, while the other is cooled indirectly through a nonreciprocal mechanical interaction. By introducing asymmetric coupling coefficients, we derived an effective non-Hermitian Hamiltonian and obtained analytical expressions for the steady-state phonon numbers. Both analytical and numerical results consistently demonstrate that increasing the nonreciprocity parameter K_g enhances directional energy transfer from the target particle to the auxiliary particle, resulting in a lower steady-state phonon number of the target particle and more efficient cooling.

The key insight gained from this study is that by introducing an auxiliary particle that interacts nonreciprocally with the target particle, one can engineer a synthetic energy flow channel that enables cooling the target particle mode to a lower effective temperature. This mechanism fundamentally differs from traditional cavity-assisted sideband cooling, as it does not solely rely on cavity dissipation but exploits the asymmetry of coupling to break detailed balance and enable directional heat transfer.

Our results provide a new perspective on controlling mechanical motion in levitated optomechanical systems through tunable nonreciprocal interactions. While demonstrated for a minimal two-particle configuration, the underlying mechanism naturally extends to larger networks, where synthetic gauge fields,[15,24] engineered dissipation,[40] or phase-controlled optical feedback[16,41] can be employed to establish spatially distributed nonreciprocal couplings. In such settings, arranging nanoparticles into unidirectional non-Hermitian chains enables cascaded energy transport and, in principle, substantially enhanced cooling performance compared with reciprocal or purely local schemes.[23,39]

From an experimental standpoint, nonreciprocal interactions in levitated optomechanics can be realized through optically mediated and phase-engineered couplings, rather than direct mechanical connections. When multiple levitated particles interact with a common optical mode or traveling optical field, effective non-Hermitian and direction-dependent mechanical interactions can emerge after eliminating the optical degrees of freedom, in close analogy with cascaded quantum systems.[15,40] Alternatively, optical phase control and feedback-assisted schemes provide flexible routes to break reciprocity without requiring magnetic fields or intrinsic time-reversal symmetry breaking.[16,41] These approaches align well with current experimental capabilities in levitated optomechanics.

The essential ingredients required for implementing such schemes including precise optical phase control, spatial-mode engineering, and tunable dissipation are already available in state-of-the-art experiments. Optical tweezers arrays and cavity-assisted trapping techniques allow accurate control over particle positions and coupling phases,[7,24] while recent demonstrations of nonreciprocal mechanical couplings further indicate that strongly asymmetric interaction regimes are experimentally accessible.[25,26] Within this framework, the proposed non-Hermitian cooling mechanism does not rely on extremely high cavity finesse, as directional energy flow rather than strong sideband resolution plays the dominant role. Several experimental challenges still remain, including maintaining phase stability, mitigating additional noise introduced by asymmetric coupling, and balancing strong nonreciprocity with overall system stability. Nevertheless, these challenges are primarily technical rather than fundamental. With continued progress in optical trapping, feedback control, and dissipation engineering, the realization of nonreciprocal cooling in levitated systems appears well within reach.

Overall, this work advances the theoretical foundation for exploiting non-Hermitian physics in levitated optomechanics and highlights its potential for scalable mechanical cooling, directional energy control, and future studies of non-equilibrium many-body dynamics in highly controllable mechanical platforms.

Appendix A: Detailed derivation of the rotating-frame transformation

In this appendix, we provide a step-by-step derivation of the transformation from the original Hamiltonian H_0 to the rotating-frame Hamiltonian H_0' discussed in Section 2. The goal is to eliminate the fast optical oscillations at the driving laser frequency $\omega_{\rm L}$, which simplifies the subsequent analysis and enables the rotating-wave approximation.

A1. Original Hamiltonian in the Schrödinger picture

We start from the non-interaction part of the Hamiltonian in the Schrödinger picture,

$$H_0 = \omega_c c^\dagger c + \omega_a a^\dagger a + \omega_b b^\dagger b, \tag{A1}$$

where ω_c is the cavity resonance frequency, and ω_a, ω_b are the mechanical oscillation frequencies of particles A and B, respectively.

A2. Transformation to the rotating frame

We introduce a unitary transformation that takes the system into a frame rotating at the driving laser frequency $\omega_{\rm L}$.

The unitary operator is defined as

$$U(t) = \exp\left[\mathrm{i}\omega_{\mathrm{L}} t\left(c^{\dagger}c\right)\right]. \tag{A2}$$

This operator acts only on the cavity mode, leaving the mechanical modes unchanged, since the driving field couples only to the cavity.

In the rotating frame, the state vector transforms as

$$|\psi_{\mathrm{rot}}(t)\rangle = U(t)|\psi(t)\rangle, \tag{A3}$$

where $|\psi(t)\rangle$ is the state in the original (Schrödinger) picture.

A3. Transformation of the Schrödinger equation

The Schrödinger equation in the original picture is

$$\mathrm{i}\frac{\partial}{\partial t}|\psi(t)\rangle = H_0|\psi(t)\rangle. \tag{A4}$$

Substituting $|\psi(t)\rangle = U^{\dagger}(t)|\psi_{\mathrm{rot}}(t)\rangle$ into Eq. (A4), we obtain

$$\mathrm{i}\frac{\partial}{\partial t}\left[U^{\dagger}(t)|\psi_{\mathrm{rot}}(t)\rangle\right] = H_0 U^{\dagger}(t)|\psi_{\mathrm{rot}}(t)\rangle. \tag{A5}$$

Expanding the left-hand side using the product rule gives

$$\begin{aligned}&\mathrm{i}\left[\left(\frac{\partial}{\partial t}U^{\dagger}(t)\right)|\psi_{\mathrm{rot}}(t)\rangle + U^{\dagger}(t)\frac{\partial}{\partial t}|\psi_{\mathrm{rot}}(t)\rangle\right]\\ &= H_0 U^{\dagger}(t)|\psi_{\mathrm{rot}}(t)\rangle.\end{aligned} \tag{A6}$$

A4. Evaluating the time derivative of $U^{\dagger}(t)$

From Eq. (A2), we have

$$U^{\dagger}(t) = \exp\left[-\mathrm{i}\omega_{\mathrm{L}} t\left(c^{\dagger}c\right)\right]. \tag{A7}$$

The time derivative is

$$\frac{\partial}{\partial t}U^{\dagger}(t) = -\mathrm{i}\omega_{\mathrm{L}}\left(c^{\dagger}c\right)U^{\dagger}(t). \tag{A8}$$

Substituting Eq. (A8) into Eq. (A6) gives

$$\begin{aligned}&\mathrm{i}\left[-\mathrm{i}\omega_{\mathrm{L}}\left(c^{\dagger}c\right)U^{\dagger}(t)|\psi_{\mathrm{rot}}(t)\rangle + U^{\dagger}(t)\frac{\partial}{\partial t}|\psi_{\mathrm{rot}}(t)\rangle\right]\\ &= H_0 U^{\dagger}(t)|\psi_{\mathrm{rot}}(t)\rangle.\end{aligned} \tag{A9}$$

Simplifying the first term: $\mathrm{i}\times(-\mathrm{i}) = 1$, so

$$\begin{aligned}&\omega_{\mathrm{L}}\left(c^{\dagger}c\right)U^{\dagger}(t)|\psi_{\mathrm{rot}}(t)\rangle + \mathrm{i}U^{\dagger}(t)\frac{\partial}{\partial t}|\psi_{\mathrm{rot}}(t)\rangle\\ &= H_0 U^{\dagger}(t)|\psi_{\mathrm{rot}}(t)\rangle.\end{aligned} \tag{A10}$$

A5. Obtaining the transformed Hamiltonian

Multiplying both sides from the left by $U(t)$ (note that $U(t)U^{\dagger}(t) = 1$), we obtain

$$\begin{aligned}&\omega_{\mathrm{L}}U(t)\left(c^{\dagger}c\right)U^{\dagger}(t)|\psi_{\mathrm{rot}}(t)\rangle + \mathrm{i}\frac{\partial}{\partial t}|\psi_{\mathrm{rot}}(t)\rangle\\ &= U(t)H_0 U^{\dagger}(t)|\psi_{\mathrm{rot}}(t)\rangle.\end{aligned} \tag{A11}$$

Rearranging to isolate the time derivative,

$$\begin{aligned}&\mathrm{i}\frac{\partial}{\partial t}|\psi_{\mathrm{rot}}(t)\rangle\\ &= \left[U(t)H_0U^{\dagger}(t) - \omega_{\mathrm{L}}U(t)\left(c^{\dagger}c\right)U^{\dagger}(t)\right]|\psi_{\mathrm{rot}}(t)\rangle.\end{aligned} \tag{A12}$$

Thus, the Hamiltonian in the rotating frame is

$$H_0' = U(t)H_0U^{\dagger}(t) - \omega_{\mathrm{L}}U(t)\left(c^{\dagger}c\right)U^{\dagger}(t). \tag{A13}$$

A6. Evaluating the transformed terms

First, we evaluate $U(t)H_0U^{\dagger}(t)$. Since $U(t)$ acts only on the cavity mode, it commutes with $a^{\dagger}a$ and $b^{\dagger}b$. Therefore,

$$U(t)H_0U^{\dagger}(t) = \omega_c U(t)c^{\dagger}cU^{\dagger}(t) + \omega_a a^{\dagger}a + \omega_b b^{\dagger}b. \tag{A14}$$

To evaluate $U(t)c^{\dagger}cU^{\dagger}(t)$, we use the Baker–Campbell–Hausdorff formula. For any operator X, Y and parameter λ,

$$\mathrm{e}^{\lambda X}Y\,\mathrm{e}^{-\lambda X} = Y + \lambda[X,Y] + \frac{\lambda^2}{2!}[X,[X,Y]] + \cdots. \tag{A15}$$

Here, $A = \mathrm{i}\omega_{\mathrm{L}}t(c^{\dagger}c)$ and $B = c^{\dagger}c$. Note that $[c^{\dagger}c, c^{\dagger}c] = 0$, so all commutators vanish. Thus,

$$U(t)c^{\dagger}cU^{\dagger}(t) = c^{\dagger}c. \tag{A16}$$

Similarly, for the second term in Eq. (A13),

$$U(t)\left(c^{\dagger}c\right)U^{\dagger}(t) = c^{\dagger}c. \tag{A17}$$

A7. Final form of the rotating-frame Hamiltonian

Substituting Eqs. (A14), (A16), and (A17) into Eq. (A13), we obtain

$$H_0' = (\omega_c - \omega_{\mathrm{L}})c^{\dagger}c + \omega_a a^{\dagger}a + \omega_b b^{\dagger}b. \tag{A18}$$

Introducing the detuning parameter $\Delta = \omega_{\mathrm{L}} - \omega_c$, we have $\omega_c - \omega_{\mathrm{L}} = -\Delta$, so

$$H_0' = -\Delta c^{\dagger}c + \omega_a a^{\dagger}a + \omega_b b^{\dagger}b. \tag{A19}$$

This is exactly the rotating-frame Hamiltonian presented in the main text. The transformation has eliminated the fast optical oscillations at frequency ω_{L}, replacing ω_c with the detuning parameter Δ.

Appendix B: Dispose of the trace-correction term

Here, we discuss the trace-correction term $\mathrm{i}\mathrm{Tr}[\rho_{\mathrm{sys}}(H_{\mathrm{eff}} - H_{\mathrm{eff}}^{\dagger})]\rho_{\mathrm{sys}}$ in Eq. (3) in the main text. Substituting $H_{\mathrm{eff}} - H_{\mathrm{eff}}^{\dagger} = 2g_2(a^{\dagger}b - ab^{\dagger})$, we obtain

$$\mathrm{i}\mathrm{Tr}[\rho_{\mathrm{sys}}(H_{\mathrm{eff}} - H_{\mathrm{eff}}^{\dagger})]\rho_{\mathrm{sys}} = 2\mathrm{i}g_2\mathrm{Tr}[\rho(a^{\dagger}b - ab^{\dagger})]\rho. \tag{B1}$$

Since particle A is coupled to the optical cavity, under the bad-cavity limit (which is satisfied by the parameters we adopt), the mode of particle A is strongly cooled and can be regarded as a small quantity α, which can be written as

$\alpha = |\alpha| e^{i\theta}$. With this approximation, Eq. (B1) can be rewritten as

$$\begin{aligned} &i\mathrm{Tr}[\rho_{\mathrm{sys}}(H_{\mathrm{eff}} - H_{\mathrm{eff}}^{\dagger})]\rho_{\mathrm{sys}} = 2ig_2\mathrm{Tr}[\rho(\alpha^* b - \alpha b^{\dagger})]\rho \\ =&2ig_2|\alpha|\mathrm{Tr}[\rho(e^{-i\theta}b - e^{i\theta}b^{\dagger})]\rho. \end{aligned} \tag{B2}$$

By introducing a phase transformation $b' = b e^{-i\theta}$, so that $b'^{\dagger} = b^{\dagger} e^{i\theta}$, Eq. (B2) can be further simplified as

$$i\mathrm{Tr}[\rho_{\mathrm{sys}}(H_{\mathrm{eff}} - H_{\mathrm{eff}}^{\dagger})]\rho_{\mathrm{sys}} = 2ig_2|\alpha|\mathrm{Tr}[\rho(b' - b'^{\dagger})]\rho. \tag{B3}$$

Noting that b and $b^{\dagger}$ are the annihilation and creation operators of particle B, we have $b - b^{\dagger} = ikp_b$, where k is a constant and p_b is the momentum operator of particle B. Under the harmonic oscillator approximation, the expectation value of p_b is zero. Because b' differs from b only by a phase factor $e^{-i\theta}$, we obtain

$$i\mathrm{Tr}[\rho_{\mathrm{sys}}(H_{\mathrm{eff}} - H_{\mathrm{eff}}^{\dagger})]\rho_{\mathrm{sys}} = 2ig_2|\alpha|\mathrm{Tr}[\rho(b' - b'^{\dagger})]\rho = 0. \tag{B4}$$

Therefore, we have demonstrated that, under the harmonic oscillator approximation and the bad-cavity limit, $i\mathrm{Tr}[\rho_{\mathrm{sys}}(H_{\mathrm{eff}} - H_{\mathrm{eff}}^{\dagger})]\rho_{\mathrm{sys}}$ vanishes.

Appendix C: Derivation of the adjoint equations for the number operators

In this appendix, we provide a complete step-by-step derivation of the adjoint equations presented in Eq. (16) of the main text. Starting from the reduced two-mode master equation, we apply perturbation theory and the Markov approximation to obtain explicit equations of motion for the phonon number operators.

C1. Decomposition of the Liouvillian

We begin by decomposing the Hamiltonian H_{A-B} into a system part and an interaction part

$$H_{\mathrm{sys}} = \omega_a a^{\dagger}a + \omega_b b^{\dagger}b, \tag{C1}$$

$$H_{\mathrm{int}} = g_{ab}ab^{\dagger} + g_{ba}a^{\dagger}b, \tag{C2}$$

where $g_{ab} = g_1 - g_2$ and $g_{ba} = g_1 + g_2$ as defined in the main text.

The total Liouvillian $\mathcal{L}'$ in Eq. (15) can be decomposed as $\mathcal{L}' = \mathcal{L}_{\mathrm{sys}} + \mathcal{L}_{\mathrm{int}}$, where

$$\mathcal{L}_{\mathrm{sys}}\rho = -i[H_{\mathrm{sys}}, \rho] + \mathcal{L}'_a\rho + \mathcal{L}_b\rho, \tag{C3}$$

$$\mathcal{L}_{\mathrm{int}}\rho = -i(H_{\mathrm{int}}\rho - \rho H_{\mathrm{int}}^{\dagger}). \tag{C4}$$

C2. Second-order perturbation expansion

Following the standard approach to open quantum systems,[29] we perform a second-order perturbative expansion of the master equation. Assuming the interaction is weak compared to the system dynamics, we obtain

$$\dot{\rho}_{a,b}(t) = \mathcal{L}_{\mathrm{sys}}\rho_{a,b}(t) + \mathcal{L}_{\mathrm{int}}\int_0^{\infty} dt' e^{\mathcal{L}_{\mathrm{sys}}t'}\mathcal{L}_{\mathrm{int}}\rho_{a,b}(t-t'). \tag{C5}$$

Here we have made the Markov approximation, extending the upper limit of the time integral to infinity and evaluating the density matrix at time t rather than $t - t'$ after the integration.[29]

C3. Expanding the interaction terms

Substituting the expression of $\mathcal{L}_{\mathrm{int}}$ from Eq. (C4) into Eq. (C5) and expanding step by step, we first obtain

$$\begin{aligned} &\mathcal{L}_{\mathrm{int}}\int_0^{\infty} dt' e^{\mathcal{L}_{\mathrm{sys}}t'}\mathcal{L}_{\mathrm{int}}\rho_{a,b}(t-t') \\ =&-iH_{\mathrm{int}}\int_0^{\infty} dt' e^{\mathcal{L}_{\mathrm{sys}}t'}\mathcal{L}_{\mathrm{int}}\rho_{a,b}(t-t') \\ &+i\int_0^{\infty} dt' e^{\mathcal{L}_{\mathrm{sys}}t'}\mathcal{L}_{\mathrm{int}}\rho_{a,b}(t-t')H_{\mathrm{int}}^{\dagger}. \end{aligned} \tag{C6}$$

Meanwhile,

$$\mathcal{L}_{\mathrm{int}}\rho_{a,b}(t-t') = -iH_{\mathrm{int}}\rho_{a,b}(t-t') + i\rho_{a,b}(t-t')H_{\mathrm{int}}^{\dagger}. \tag{C7}$$

C4. Transformation to the Heisenberg picture and Markov approximation

To simplify these expressions, we transform to the Heisenberg picture. The key insight is that the action of $e^{\mathcal{L}_{\mathrm{sys}}t'}$ on an operator O corresponds to evolving that operator under the adjoint Liouvillian $\mathcal{L}_{\mathrm{sys}}^{\dagger}$:[29]

$$e^{\mathcal{L}_{\mathrm{sys}}t'}(O\rho) = (e^{\mathcal{L}_{\mathrm{sys}}^{\dagger}t'}O)\rho, \tag{C8}$$

where we have used the Markov approximation to replace $\rho(t-t')$ with $\rho(t)$ inside the integral. This is valid when the correlation time of the bath is much shorter than the timescale of system dynamics.

Applying this relation, we obtain

$$\begin{aligned} &e^{\mathcal{L}_{\mathrm{sys}}t'}\mathcal{L}_{\mathrm{int}}\rho_{a,b}(t-t') \\ =&-ie^{\mathcal{L}_{\mathrm{sys}}^{\dagger}t'}(H_{\mathrm{int}})\rho_{a,b}(t) + i\rho_{a,b}(t)e^{\mathcal{L}_{\mathrm{sys}}^{\dagger}t'}(H_{\mathrm{int}}^{\dagger}). \end{aligned} \tag{C9}$$

Substituting Eqs. (C7) and (C9) into Eq. (C6) and collecting terms, the reduced master equation can be written as

$$\begin{aligned} \dot{\rho}_{a,b}(t) =& -i[H_{\mathrm{sys}}, \rho_{a,b}(t)] \\ &-\int_0^{\infty} dt' H_{\mathrm{int}}e^{\mathcal{L}_{\mathrm{sys}}^{\dagger}t'}(H_{\mathrm{int}})\rho_{a,b}(t) \\ &+\int_0^{\infty} dt' H_{\mathrm{int}}\rho_{a,b}(t)e^{\mathcal{L}_{\mathrm{sys}}^{\dagger}t'}(H_{\mathrm{int}}^{\dagger}) \\ &+\int_0^{\infty} dt' e^{\mathcal{L}_{\mathrm{sys}}^{\dagger}t'}(H_{\mathrm{int}})\rho_{a,b}(t)H_{\mathrm{int}}^{\dagger} \\ &-\int_0^{\infty} dt' \rho_{a,b}(t)e^{\mathcal{L}_{\mathrm{sys}}^{\dagger}t'}(H_{\mathrm{int}}^{\dagger})H_{\mathrm{int}}^{\dagger} \\ &+\mathcal{L}'_a\rho_{a,b}(t) + \mathcal{L}_b\rho_{a,b}(t). \end{aligned} \tag{C10}$$

C5. Evaluating the adjoint evolution of $H_{\rm int}$

We now need to compute $\mathrm{e}^{\mathcal{L}^\dagger_{\rm sys}t'}(H_{\rm int})$ and $\mathrm{e}^{\mathcal{L}^\dagger_{\rm sys}t'}(H^\dagger_{\rm int})$. First, we express $H_{\rm int}$ in terms of its components

$$\begin{aligned}\mathrm{e}^{\mathcal{L}^\dagger_{\rm sys}t'}(H_{\rm int}) &= (g_1+g_2)(\mathrm{e}^{\mathcal{L}^\dagger_{\rm sys}t'}a^\dagger)(\mathrm{e}^{\mathcal{L}^\dagger_{\rm sys}t'}b)\\ &\quad+(g_1-g_2)(\mathrm{e}^{\mathcal{L}^\dagger_{\rm sys}t'}a)(\mathrm{e}^{\mathcal{L}^\dagger_{\rm sys}t'}b^\dagger).\end{aligned}\tag{C11}$$

The action of $\mathcal{L}^\dagger_{\rm sys}$ on a is derived as follows. For any operator O, the adjoint Liouvillian is defined by $\mathrm{Tr}[O(\mathcal{L}_{\rm sys}\rho)] = \mathrm{Tr}[(\mathcal{L}^\dagger_{\rm sys}O)\rho]$. For the harmonic oscillator with damping, we have the well-known result[29]

$$\mathcal{L}^\dagger_{\rm sys}a = \mathrm{i}[H_{\rm sys},a]+\mathcal{L}'^\dagger_a a+\mathcal{L}^\dagger_b a.\tag{C12}$$

Computing each term explicitly:

$$\mathrm{i}[H_{\rm sys},a] = \mathrm{i}[\omega_a a^\dagger a,a] = -\mathrm{i}\omega_a a,\tag{C13}$$

$$\begin{aligned}\mathcal{L}'^\dagger_a a &= (1+\bar{n}'_a)\kappa'_a(2a^\dagger aa-a^\dagger aa-aa^\dagger a)\\ &\quad+\bar{n}'_a\kappa'_a(2aaa^\dagger-aa^\dagger a-aaa^\dagger)\\ &= -(1+\bar{n}'_a)\kappa'_a a+\bar{n}'_a\kappa'_a a = -\kappa'_a a,\end{aligned}\tag{C14}$$

$$\mathcal{L}^\dagger_b a = 0 \quad (\text{since } \mathcal{L}_b \text{ acts only on mode } b).\tag{C15}$$

Combining these results, we obtain

$$\mathcal{L}^\dagger_{\rm sys}a = -(\mathrm{i}\omega_a+\kappa'_a)a.\tag{C16}$$

This is a key result: under the adjoint Liouvillian, the annihilation operator decays exponentially with rate κ'_a and oscillates at frequency ω_a.

Solving the differential equation $\mathrm{d}a(t')/\mathrm{d}t' = \mathcal{L}^\dagger_{\rm sys}a(t')$ with initial condition $a(0)=a$, we get

$$\mathrm{e}^{\mathcal{L}^\dagger_{\rm sys}t'}a = \mathrm{e}^{-(\kappa'_a+\mathrm{i}\omega_a)t'}a.\tag{C17}$$

Similarly, we derive

$$\mathrm{e}^{\mathcal{L}^\dagger_{\rm sys}t'}a^\dagger = \mathrm{e}^{-(\kappa'_a-\mathrm{i}\omega_a)t'}a^\dagger,\tag{C18}$$

$$\mathrm{e}^{\mathcal{L}^\dagger_{\rm sys}t'}b = \mathrm{e}^{-(\kappa_b+\mathrm{i}\omega_b)t'}b,\tag{C19}$$

$$\mathrm{e}^{\mathcal{L}^\dagger_{\rm sys}t'}b^\dagger = \mathrm{e}^{-(\kappa_b-\mathrm{i}\omega_b)t'}b^\dagger.\tag{C20}$$

C6. Substituting back into $H_{\rm int}$

Substituting these relations into Eq. (C11), we obtain

$$\begin{aligned}\mathrm{e}^{\mathcal{L}^\dagger_{\rm sys}t'}(H_{\rm int}) &= (g_1+g_2)\,\mathrm{e}^{-\left((\kappa'_a+\kappa_b)-\mathrm{i}(\omega_a-\omega_b)\right)t'}a^\dagger b\\ &\quad+(g_1-g_2)\,\mathrm{e}^{-\left((\kappa'_a+\kappa_b)+\mathrm{i}(\omega_a-\omega_b)\right)t'}ab^\dagger,\end{aligned}\tag{C21}$$

where we have neglected fast-oscillating terms such as a^2 and $a^{\dagger 2}$ that do not conserve energy in the rotating wave approximation.

Similarly, for the Hermitian conjugate:

$$\begin{aligned}\mathrm{e}^{\mathcal{L}^\dagger_{\rm sys}t'}(H^\dagger_{\rm int}) &= (g_1+g_2)\,\mathrm{e}^{-\left((\kappa'_a+\kappa_b)+\mathrm{i}(\omega_a-\omega_b)\right)t'}ab^\dagger\\ &\quad+(g_1-g_2)\,\mathrm{e}^{-\left((\kappa'_a+\kappa_b)-\mathrm{i}(\omega_a-\omega_b)\right)t'}a^\dagger b.\end{aligned}\tag{C22}$$

C7. Performing the time integrals

For the remainder of this derivation, we set $\omega_a=\omega_b$, which is the regime considered in our numerical simulations. This simplifies the exponents by eliminating the oscillatory terms $\mathrm{e}^{\pm\mathrm{i}(\omega_a-\omega_b)t'}$.

The time integrals in Eq. (C10) are now straightforward to evaluate using $\int_0^\infty \mathrm{e}^{-(\kappa'_a+\kappa_b)t'}\mathrm{d}t' = 1/(\kappa'_a+\kappa_b)$.

First, consider the term $-\int_0^\infty \mathrm{d}t' H_{\rm int}\,\mathrm{e}^{\mathcal{L}^\dagger_{\rm sys}t'}(H_{\rm int})\rho_{a,b}(t)$. Using Eqs. (C6) and (C21):

$$\begin{aligned}&-\int_0^\infty \mathrm{d}t' H_{\rm int}\,\mathrm{e}^{\mathcal{L}^\dagger_{\rm sys}t'}(H_{\rm int})\rho_{a,b}(t)\\ &= -\int_0^\infty \mathrm{d}t'\Big((g_1-g_2)ab^\dagger+(g_1+g_2)a^\dagger b\Big)\\ &\quad\times\Big((g_1+g_2)\,\mathrm{e}^{-(\kappa'_a+\kappa_b)t'}a^\dagger b\\ &\quad+(g_1-g_2)\,\mathrm{e}^{-(\kappa'_a+\kappa_b)t'}ab^\dagger\Big)\rho_{a,b}(t)\\ &= -\frac{g_1^2-g_2^2}{\kappa'_a+\kappa_b}(aa^\dagger b^\dagger b+a^\dagger abb^\dagger)\rho_{a,b}(t),\end{aligned}\tag{C23}$$

where we have used the commutation relations $[a,a^\dagger]=1$ and $[b,b^\dagger]=1$ to simplify the operator products.

Following similar procedures for the remaining terms in Eq. (C10), we obtain

$$\begin{aligned}&\int_0^\infty \mathrm{d}t' H_{\rm int}\rho_{a,b}(t)\,\mathrm{e}^{\mathcal{L}^\dagger_{\rm sys}t'}(H^\dagger_{\rm int})\\ &= \frac{1}{\kappa'_a+\kappa_b}\Big((g_1-g_2)^2ab^\dagger\rho_{a,b}(t)a^\dagger b\\ &\quad+(g_1+g_2)^2a^\dagger b\rho_{a,b}(t)ab^\dagger\Big),\end{aligned}\tag{C24}$$

$$\begin{aligned}&\int_0^\infty \mathrm{d}t'\,\mathrm{e}^{\mathcal{L}^\dagger_{\rm sys}t'}(H_{\rm int})\rho_{a,b}(t)H^\dagger_{\rm int}\\ &= \frac{1}{\kappa'_a+\kappa_b}\Big((g_1+g_2)^2a^\dagger b\rho_{a,b}(t)ab^\dagger\\ &\quad+(g_1-g_2)^2ab^\dagger\rho_{a,b}(t)a^\dagger b\Big),\end{aligned}\tag{C25}$$

$$\begin{aligned}&-\int_0^\infty \mathrm{d}t'\rho_{a,b}(t)\,\mathrm{e}^{\mathcal{L}^\dagger_{\rm sys}t'}(H^\dagger_{\rm int})H^\dagger_{\rm int}\\ &= -\frac{g_1^2-g_2^2}{\kappa'_a+\kappa_b}\rho_{a,b}(t)(a^\dagger abb^\dagger+aa^\dagger b^\dagger b).\end{aligned}\tag{C26}$$

C8. The final reduced master equation

Substituting Eqs. (C23)–(C26) into Eq. (C10) and collecting terms, we obtain the reduced master equation in Lindblad form

$$\begin{aligned}\dot{\rho}_{a,b}(t) &= -\mathrm{i}\left[H'_{\rm sys}+\frac{4g_2^2}{\kappa'_a+\kappa_b}a^\dagger ab^\dagger b,\rho_{a,b}(t)\right]\\ &\quad+\mathcal{L}'_a\rho_{a,b}(t)+\mathcal{L}_b\rho_{a,b}(t)+\mathcal{L}_{ab}\rho_{a,b}(t),\end{aligned}\tag{C27}$$

where the modified system Hamiltonian $H'_{\rm sys}$ is given by

$$\begin{aligned}H'_{\rm sys} &= \left(\omega_a+\frac{2g_2^2-2g_1g_2}{\kappa'_a+\kappa_b}\right)a^\dagger a\\ &\quad+\left(\omega_b+\frac{2g_2^2+2g_1g_2}{\kappa'_a+\kappa_b}\right)b^\dagger b,\end{aligned}\tag{C28}$$

and the additional Liouvillian describing the nonreciprocal interaction is

$$\mathcal{L}_{ab} = \frac{(g_1+g_2)^2}{\kappa_a'+\kappa_b} D_{a^\dagger b} + \frac{(g_1-g_2)^2}{\kappa_a'+\kappa_b} D_{ab^\dagger}. \tag{C29}$$

C9. Derivation of the adjoint equations for phonon numbers

The adjoint master equation describes the time evolution of operators in the Heisenberg picture. For any operator O, the adjoint Liouvillian $\mathcal{L}^\dagger$ satisfies $\mathrm{Tr}[O(\mathcal{L}\rho)] = \mathrm{Tr}[(\mathcal{L}^\dagger O)\rho]$, which implies $\mathrm{d}\langle O\rangle/\mathrm{d}t = \langle \mathcal{L}^\dagger O\rangle$.[29]

Applying this to the phonon number operators $n_a = a^\dagger a$ and $n_b = b^\dagger b$, we have

$$\frac{\mathrm{d}}{\mathrm{d}t}\langle n_a\rangle = \langle \mathcal{L}^\dagger n_a\rangle = \langle (\mathcal{L}_{ab}^\dagger + \mathcal{L}_a'^\dagger + \mathcal{L}_b^\dagger) n_a\rangle, \tag{C30}$$

$$\frac{\mathrm{d}}{\mathrm{d}t}\langle n_b\rangle = \langle \mathcal{L}^\dagger n_b\rangle = \langle (\mathcal{L}_{ab}^\dagger + \mathcal{L}_a'^\dagger + \mathcal{L}_b^\dagger) n_b\rangle. \tag{C31}$$

Note that $\mathcal{L}_b^\dagger n_a = 0$ and $\mathcal{L}_a'^\dagger n_b = 0$ since these Liouvillians act on different modes.

To evaluate these expressions, we need the action of each adjoint Lindblad operator on n_a and n_b. For a general Lindblad dissipator $D_x = 2x\rho x^\dagger - x^\dagger x\rho - \rho x^\dagger x$, the adjoint action on an operator O is given by[29]

$$D_x^\dagger O = 2x^\dagger O x - x^\dagger x O - O x^\dagger x. \tag{C32}$$

Applying this formula, we compute

$$\begin{aligned} D_{a^\dagger b}^\dagger(n_a) &= 2(ab^\dagger)n_a(a^\dagger b) - (ab^\dagger)(a^\dagger b)n_a - n_a(ab^\dagger)(a^\dagger b) \\ &= 2(1+n_a)n_b, \end{aligned} \tag{C33}$$

$$\begin{aligned} D_{ab^\dagger}^\dagger(n_a) &= 2(a^\dagger b)n_a(ab^\dagger) - (a^\dagger b)(ab^\dagger)n_a - n_a(a^\dagger b)(ab^\dagger) \\ &= -2n_a(1+n_b), \end{aligned} \tag{C34}$$

$$\begin{aligned} D_a^\dagger(n_a) &= 2a^\dagger n_a a - a^\dagger a n_a - n_a a^\dagger a \\ &= -2n_a, \end{aligned} \tag{C35}$$

$$\begin{aligned} D_{a^\dagger}^\dagger(n_a) &= 2a n_a a^\dagger - a a^\dagger n_a - n_a a a^\dagger \\ &= 2(1+n_a). \end{aligned} \tag{C36}$$

Similarly for n_b:

$$\begin{aligned} D_{a^\dagger b}^\dagger(n_b) &= 2(ab^\dagger)n_b(a^\dagger b) - (ab^\dagger)(a^\dagger b)n_b - n_b(ab^\dagger)(a^\dagger b) \\ &= -2(1+n_a)n_b, \end{aligned} \tag{C37}$$

$$\begin{aligned} D_{ab^\dagger}^\dagger(n_b) &= 2(a^\dagger b)n_b(ab^\dagger) - (a^\dagger b)(ab^\dagger)n_b - n_b(a^\dagger b)(ab^\dagger) \\ &= 2n_a(1+n_b), \end{aligned} \tag{C38}$$

$$\begin{aligned} D_b^\dagger(n_b) &= 2b^\dagger n_b b - b^\dagger b n_b - n_b b^\dagger b \\ &= -2n_b, \end{aligned} \tag{C39}$$

$$\begin{aligned} D_{b^\dagger}^\dagger(n_b) &= 2b n_b b^\dagger - b b^\dagger n_b - n_b b b^\dagger \\ &= 2(1+n_b). \end{aligned} \tag{C40}$$

C10. Final equations of motion

Substituting these results into Eqs. (C30)–(C31) and including the explicit coefficients from Eq. (C29), we obtain

$$\begin{aligned} \frac{\mathrm{d}}{\mathrm{d}t}n_a &= \frac{(g_1+g_2)^2}{\kappa_a'+\kappa_b} D_{a^\dagger b}^\dagger(n_a) + \frac{(g_1-g_2)^2}{\kappa_a'+\kappa_b} D_{ab^\dagger}^\dagger(n_a) \\ &\quad + (1+\bar{n}_a')\kappa_a' D_a^\dagger(n_a) + \bar{n}_a'\kappa_a' D_{a^\dagger}^\dagger(n_a), \end{aligned} \tag{C41}$$

$$\begin{aligned} \frac{\mathrm{d}}{\mathrm{d}t}n_b &= \frac{(g_1+g_2)^2}{\kappa_a'+\kappa_b} D_{a^\dagger b}^\dagger(n_b) + \frac{(g_1-g_2)^2}{\kappa_a'+\kappa_b} D_{ab^\dagger}^\dagger(n_b) \\ &\quad + (1+\bar{n}_b)\kappa_b D_b^\dagger(n_b) + \bar{n}_b\kappa_b D_{b^\dagger}^\dagger(n_b). \end{aligned} \tag{C42}$$

Finally, inserting the explicit forms from Eqs. (C33)–(C40) and taking expectation values, we arrive at the form given in Eq. (16) presented in the main text. In the final step, we have applied the mean-field approximation $\langle n_a n_b\rangle = \langle n_a\rangle\langle n_b\rangle$, which is valid in the limit of weak correlations between the two modes.

Appendix D: Stationary state for the average phonon number of particle A

Similar to Eq. (17) in the main text, the stationary state for the average phonon number of particle A can be solved from a quadratic equation written as

$$D\langle n_a\rangle^2 + E\langle n_a\rangle + F = 0, \tag{D1}$$

where

$$D = -\frac{8g_1g_2\kappa_a'}{\kappa_b(\kappa_a'+\kappa_b)}, \tag{D2a}$$

$$\begin{aligned} E &= \frac{8g_1g_2}{\kappa_a'+\kappa_b}\left(\frac{\kappa_a'}{\kappa_b}\bar{n}_a' + \bar{n}_b\right) \\ &\quad - \frac{2(g_1+g_2)^2}{\kappa_a'+\kappa_b}\cdot\frac{\kappa_a'}{\kappa_b} - \frac{2(g_1-g_2)^2}{\kappa_a'+\kappa_b} - \kappa_a', \end{aligned} \tag{D2b}$$

$$F = \frac{2(g_1+g_2)^2}{\kappa_a'+\kappa_b}\left(\frac{\kappa_a'}{\kappa_b}\bar{n}_a' + \bar{n}_b\right) + \kappa_a'\bar{n}_a'. \tag{D2c}$$

Acknowledgements

This work is supported by the National Natural Science Foundation of China (Grant No. 12441502) and the Beijing Institute of Technology Research Fund Program (Grant No. 2024CX01015).

References

[1] Aspelmeyer M, Kippenberg T J and Marquardt F 2014 *Rev. Mod. Phys.* **86** 1391
[2] Kippenberg T J and Vahala K J 2008 *Science* **321** 1172
[3] Delić U, Reisenbauer M, Dare K, Grass D, Vuletić V, Kiesel N and Aspelmeyer M 2020 *Science* **367** 892
[4] Chan J, Alegre T M, Safavi-Naeini A H, Hill J T, Krause A, Gröblacher S, Aspelmeyer M and Painter O 2011 *Nature* **478** 89
[5] Gieseler J, Novotny L and Quidant R 2013 *Nat. Phys.* **9** 806
[6] Millen J, Monteiro T S, Pettit R and Vamivakas A N 2020 *Reports on Progress in Physics* **83** 026401

[7] Barker P and Shneider M 2010 *Phys. Rev. A* **81** 023826
[8] Gonzalez-Ballestero C, Maurer P, Windey D, Novotny L, Reimann R and Romero-Isart O 2019 *Phys. Rev. A* **100** 013805
[9] Gieseler J, Deutsch B, Quidant R and Novotny L 2012 *Phys. Rev. Lett.* **109** 103603
[10] Anetsberger G, Arcizet O, Unterreithmeier Q P, Riviere R, Schliesser A, Weig E M, Kotthaus J P and Kippenberg T J 2009 *Nat. Phys.* **5** 909
[11] Martin I, Shnirman A, Tian L and Zoller P 2004 *Phys. Rev. B* **69** 125339
[12] Wilson-Rae I, Nooshi N, Zwerger W and Kippenberg T J 2007 *Phys. Rev. Lett.* **99** 093901
[13] Mari A and Eisert J 2012 *Phys. Rev. Lett.* **108** 120602
[14] Ma Y, Yin Z q, Huang P, Yang W and Du J 2016 *Phys. Rev. A* **94** 053836
[15] Metelmann A and Clerk A A 2015 *Phys. Rev. X* **5** 021025
[16] Ruesink F, Miri M A, Alu A and Verhagen E 2016 *Nat. Commun.* **7** 13662
[17] Regensburger A, Bersch C, Miri M A, Onishchukov G, Christodoulides D N and Peschel U 2012 *Nature* **488** 167
[18] Chen W, Kaya Özdemir Ş, Zhao G, Wiersig J and Yang L 2017 *Nature* **548** 192
[19] Liu S, Yin Z Q and Li T 2020 *Advanced Quantum Technologies* **3** 1900099
[20] Feng L, El-Ganainy R and Ge L 2017 *Nat. Photonics* **11** 752
[21] Doppler J, Mailybaev A A, Böhm J, Kuhl U, Girschik A, Libisch F, Milburn T J, Rabl P, Moiseyev N and Rotter S 2016 *Nature* **537** 76
[22] El-Ganainy R, Makris K G, Khajavikhan M, Musslimani Z H, Rotter S and Christodoulides D N 2018 *Nat. Phys.* **14** 11
[23] Xu H, Delić U, Wang G, Li C, Cappellaro P and Li J 2024 *Phys. Rev. Lett.* **132** 110402
[24] Wang C, Fu Z, Mao W, Qie J, Stone A D and Yang L 2023 *Advances in Optics and Photonics* **15** 442
[25] Reisenbauer M, Rudolph H, Egyed L, Hornberger K, Zasedatelev A V, Abuzarli M, Stickler B A and Delić U 2024 *Nat. Phys.* **20** 1629
[26] Liška V, Zemánková T, Jákl P, Šiler M, Simpson S H, Zemánek P and Brzobohatỳ O 2024 *Nat. Phys.* **20** 1622
[27] Liu Y C, Hu Y W, Wong C W and Xiao Y F 2013 *Chin. Phys. B* **22** 114213
[28] Clerk A A, Devoret M H, Girvin S M, Marquardt F and Schoelkopf R J 2010 *Rev. Mod. Phys.* **82** 1155
[29] Gardiner C and Zoller P 2004 *Quantum Noise* (Springer)
[30] Barzanjeh S, Xuereb A, Alù A, Mann S A, Nefedkin N, Peano V and Rabl P 2025 arXiv: 2508.03945
[31] Breuer H P and Petruccione F 2002 *The Theory of Open Quantum Systems* (Oxford University Press)
[32] Johansson J R, Nation P D and Nori F 2012 *Computer Physics Communications* **183** 1760
[33] Manzano D 2020 *Aip Advances* **10** 025106
[34] Schack R and Brun T A 1997 *Computer Physics Communications* **102** 210
[35] Rivas Á, Huelga S F and Plenio M B 2014 *Reports on Progress in Physics* **77** 094001
[36] Prosen T 2008 *New J. Phys.* **10** 043026
[37] White S R and Feiguin A E 2004 *Phys. Rev. Lett.* **93** 076401
[38] Barnett S and Radmore P M 2002 *Methods in theoretical quantum optics* Vol. 15 (Oxford University Press)
[39] Ashida Y, Gong Z and Ueda M 2020 *Advances in Physics* **69** 249
[40] Metelmann A and Clerk A 2014 *Phys. Rev. Lett.* **112** 133904
[41] Kippenberg T, Rokhsari H, Carmon T, Scherer A and Vahala K 2005 *Phys. Rev. Lett.* **95** 033901
[42] Marago O M, Jones P H, Gucciardi P G, Volpe G and Ferrari A C 2013 *Nat. Nanotechnol.* **8** 807